Available online at www.sciencedirect.com

SciVerse ScienceDirect

Procedia Engineering 00 (2012) 000–000

Procedia Engineering

www.elsevier.com/locate/procedia

The 12th Hypervelocity Impact Symposium

Ejecta size distribution resulting from hypervelocity impact of spherical projectiles on CFRP laminates

Masahiro Nishida[a,*], Hiroaki Kato[a], Koichi Hayashi[a], Masumi Higashide[b]

[a]*Nagoya Institute of Technology, Gokiso-cho, Showa-ku, Nagoya 466-8555, Japan*
[b]*Japan Aerospace Exploration Agency, Aerospace Research and Development Directorate, 7-44-1, Jindaiji Higashimachi, Chofu, Tokyo 182-8522, Japan*

Abstract

The size distributions of ejecta resulting from projectile perforation of CFRP (carbon fiber reinforced plastic) laminates were examined. The shape of the ejecta cone and the debris cloud was observed using a high-speed video camera. The ejecta fragments were collected from the test chamber after impact experiments. The number of fragments ejected on the front side of the target was altered by the impact velocity. Conversely, regardless of impact velocity, the number of fragments ejected on the rear side of the target was almost the same. The results were also compared with the results of NASA's breakup model. The slope on the cumulative number distribution curve of characteristic length, L_C, was almost the same as that of NASA's breakup model. The area-to-mass ratio distribution of ejecta fragments from CFRP laminates ranged within and above the area surrounded by ±3σ of NASA's breakup model.

Keywords: Ejecta fragment size, CFRP laminates, Aluminum alloy projectiles, Hypervelocity impact, Projectile perforation

1. Introduction

Space debris orbits the Earth at velocities of over several kilometers per second, and often strikes spacecraft, satellites, and space stations. The International Space Station employs shields such as the Whipple bumper to protect itself against space debris. When space debris strikes or perforates the shields of space stations or the outer surfaces of spacecraft and space stations, fragments from the shields and the outer surfaces are ejected, and these fragments of space debris are widely scattered. These fragments (ejected materials) become new debris, as pointed out by Murr and co-workers [1]. The international standardization of test procedures to evaluate spacecraft material ejecta is being promoted [2]. Many studies have been conducted on related phenomena [3, 4]. The use of CFRP (carbon fiber reinforced plastic) laminates in satellites has been increasing recently, and several attempts to investigate the ballistic behavior of CFRP laminates including debris clouds, [5-10] have been reported concerning the ballistic limit, perforation behavior and debris clouds when projectiles have perforated the CFRP laminates at high velocities. Numerical material models that predict the highly dynamic behavior of CFRP under hypervelocity impact were examined [11]. However, the size distributions of fragments ejected from CFRP laminates have not yet been fully elucidated.

We examined size distributions of ejecta resulting from projectile perforation of CFRP laminates. The shape of the ejecta cone and the debris cloud was observed using a high-speed video camera, and the ejecta were collected from the test chamber after the impact experiments. The ejecta fragments collected from areas in front of and behind the targets were compared. The number of fragments ejected on the front side of the targets was altered by the impact velocity. Conversely, regardless of impact velocity, the number of ejecta fragments ejected on the rear side of the targets was approximately the

* Corresponding author. Tel.: +81-52-735-5349 ; fax: +81-52-735-5342 .
E-mail address: nishida.masahiro@nitech.ac.jp .

same. The results were also compared with the results of NASA's breakup model. The slope on the cumulative number distribution curve of characteristic length, L_C, was almost the same as that of NASA's breakup model. The area-to-mass ratio distribution of ejecta fragments from CFRP laminates ranged within and above the area surrounded by ±3σ of NASA's breakup model.

2. Experimental Methods

We employed CFRP laminates consisting of epoxy-based carbon fiber UD pre-pregs (IMS60/#133, Toho Tenax Co. Ltd.) as a target material. The size of the CFRP laminates was 150×100 mm, with thickness of 3.4 mm, and the constitution of the CFRP laminates was $[+45°/0°/–45°/90°]_{3S}$ (24 ply). Projectiles with a diameter of 7 mm made of aluminum alloy (2017-T4) were used. A two-stage light-gas gun at Nagoya Institute of Technology was used to accelerate the projectiles with a sabot at the CFRP laminate targets. The impact velocities were 0.9 to 2.8 km/s. Front and rear witness plates (200 mm × 200 mm, 2 mm in thickness) with a hole of 25 mm made of copper, C1100P-1/4H, were placed 50 mm in front of and behind each target as shown in Fig. 1 to determine the scattering area. In order to examine impact craters impacted by the ejecta fragments from the targets, witness plates with a hole were used. In the case that rear witness plates do not have a hole, rear witness plates would be largely deformed and it is difficult to observe impact craters. When the forward ejecta and backward ejecta coming from the target were separately collected, the space between the target and the rear witness plate was surrounded by plates. The ejecta debris immediately after impact was observed using a high-speed video camera (nac Image Technology Inc., ULTRA Cam HS-106E).

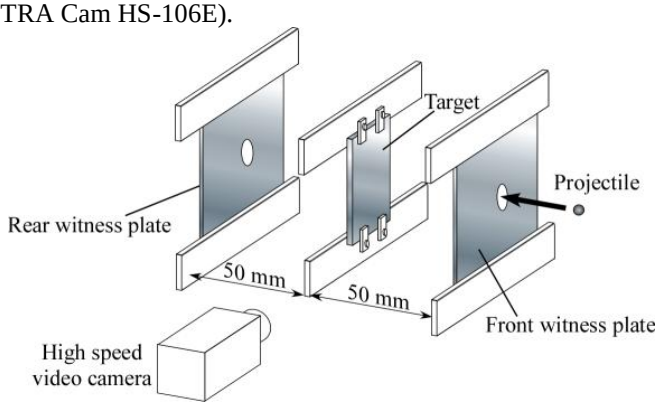

Fig. 1. Experimental setup for hypervelocity impact.

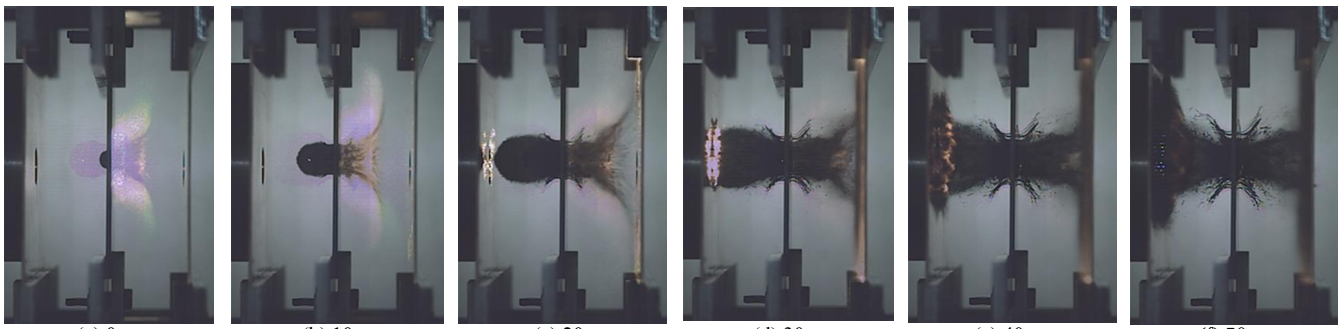

(a) 0 μs (b) 10 μs (c) 20 μs (d) 30 μs (e) 40 μs (f) 50 μs

Fig. 2. High-speed video camera photographs of scattering ejecta (2.80 km/s).

3. Results and Discussion

3.1. Observation of ejecta using high-speed video camera photographs

Fig. 2 shows high-speed video camera photographs of scattering ejecta after impact at an impact velocity of 2.80 km/s. Just after impact, the ejecta cone was formed in front of the target and the debris cloud was formed behind the target. The ejecta cone and the debris cloud struck the front witness plate and the rear witness plate respectively, slightly more than 20 μs after impact. The tip speeds of the ejecta cone and the debris cloud were almost the same and were approximately 2.3-2.5 km/s, which was slightly below the impact velocity of the projectile. At 30 μs, large fragments were observed.

3.2. Observation of the target after impact

Fig. 3 shows the CFPR laminate after impact. It was found that the outer layers with the same width as the diameter of perforation hole had peeled off along the fiber direction (+45°direction). The large fragments observed at 30 μs on the high-speed video camera photograph seem to be the fragments that peeled off from the outer layers. The hole produced by the projectile impact was roughly circular in shape. Fig. 4 shows the CFRP laminates after impact when the space between the target and the rear witness plate was surrounded by plates. At 0.9 km/s, a small part of outer layer on the front side was peeled off. Even though the impact velocity was low, a large area stretching from the right to the left edges of the target was peeled off on the rear side of the target. At 2.82 km/s, large areas on the front and rear sides of the target were peeled off. The impact velocity affected the peel-off area on the front side of the target. On the other hand, the peel-off area on the rear side of the target did not depend on the impact velocity. It can be seen from Fig. 3 and Fig. 4(b) that the outward appearance of the targets was the same, regardless of whether the space between the target and the rear witness plate was surrounded by plates or not. White *et al.* [12] examined the behavior of a CFRP (0°/90°, 4 mm) subject to projectile impact of 2 mm aluminum spheres at 6 km/s. The hole produced by the projectile impact was roughly circular in shape. The area peeled off on the rear side of the target was smaller than that of the front side. This tendency was different from our results.

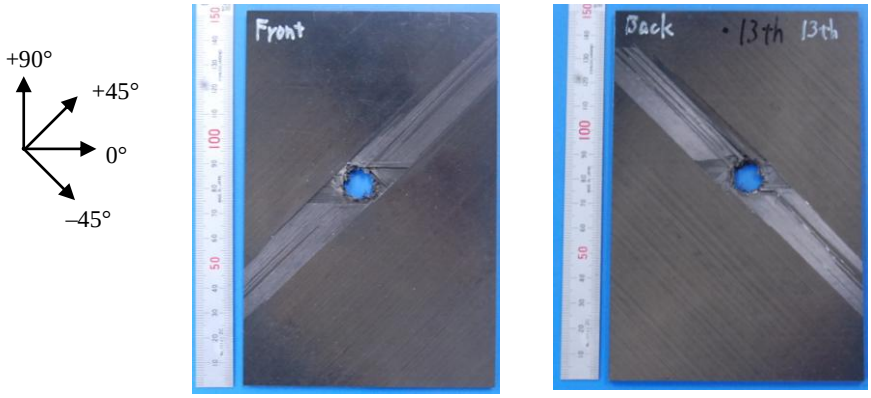

(a) Front side (b) Rear side

Fig. 3. Photographs of CFPR laminate after impact (2.80 km/s).

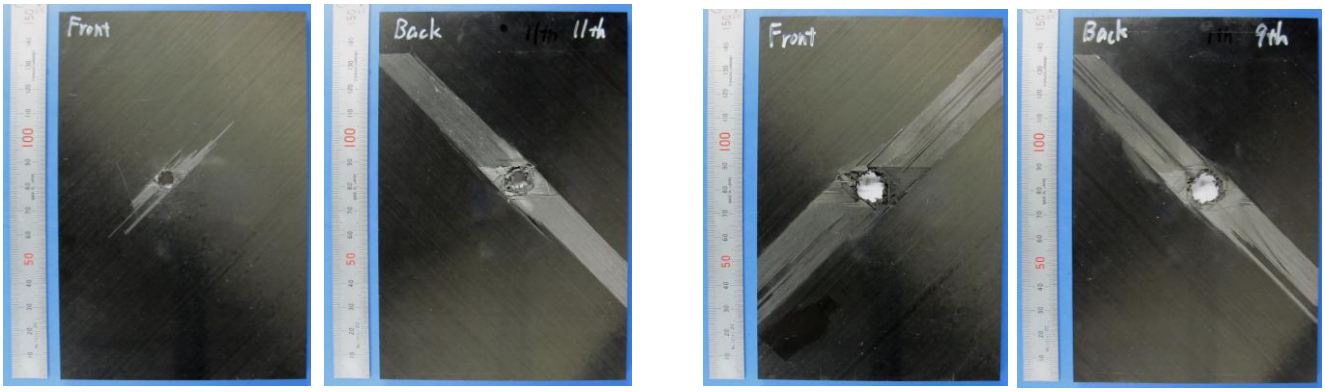

(a-1) Front side (a-2) Rear side (b-1) Front side (b-2) Rear side

(a) 0.90 km/s (b) 2.82 km/s

Fig. 4. Effect of impact velocity on damage to CFPR laminate.

3.3. Observation of front and rear witness plates

Fig. 5 shows photographs of the witness plates after impact at 2.80 km/s. Many elongated craters created by ejecta fragments on the front witness plate can be observed. A ring consisting of many craters can be observed on the front witness plate as well as the ejecta ring created by the ejecta cone when the spherical projectiles struck the thick targets [13]. On the rear witness plate, a black and circular area consisting of many craters was observed. Fig. 6 shows the witness plates after impact when the space between the target and the rear witness plate was surrounded by plates. The craters on the front

witness plate and the rear witness plate became clearer with increasing impact velocity. The circular area on the rear witness plate became blacker with increasing impact velocity. It can be seen from Fig. 5 and Fig. 6(b) that the craters of the witness plates were the same, regardless of whether the space between the target and the rear witness plate was surrounded by plates or not.

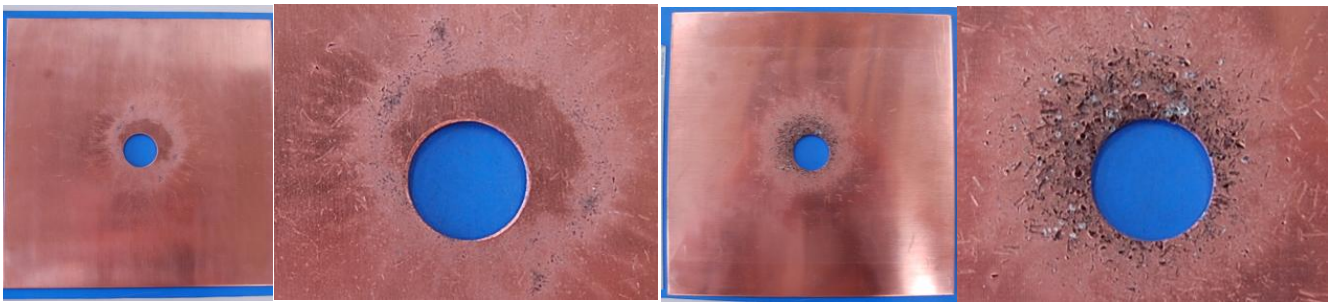

(a) Front side (b) Enlargement of Fig. (a) (c) Rear side (d) Enlargement of Fig. (c)

Fig. 5. Photographs of witness plates after impact (2.80 km/s).

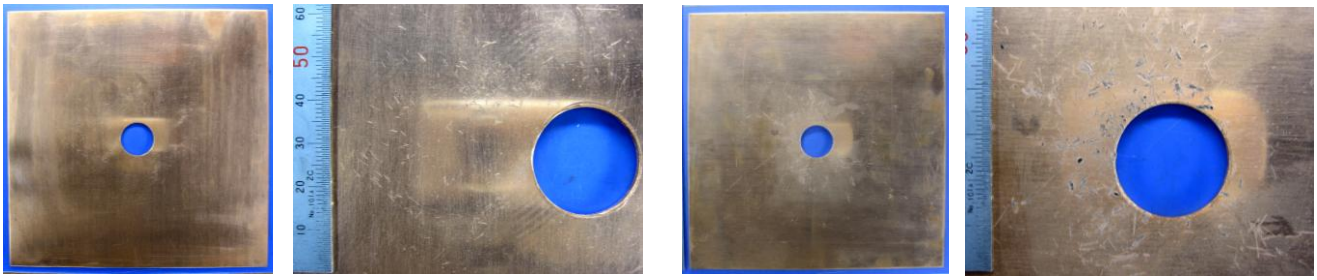

(a-1) Front side (a-2) Enlargement of (a-1) (a-3) Rear side (a-4) Enlargement of (a-3)

(a) 1.39 km/s

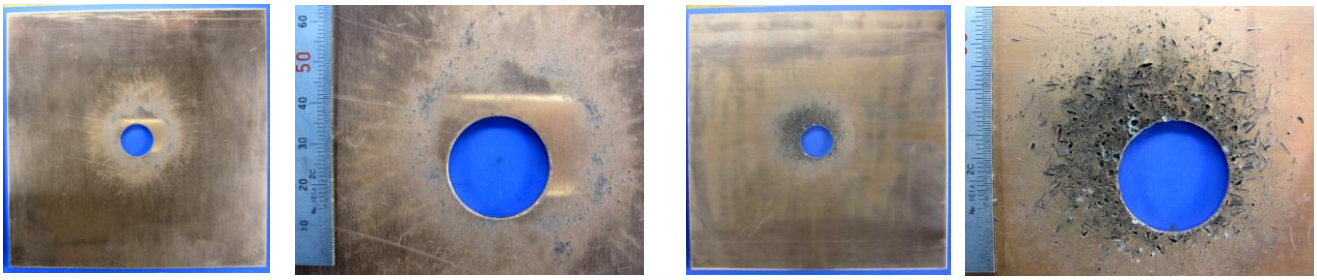

(b-1) Front side (b-2) Enlargement of (b-1) (b-3) Rear side (b-4) Enlargement of (b-3)

(b) 2.82 km/s

Fig. 6. Effect of impact velocity on crater of witness plates.

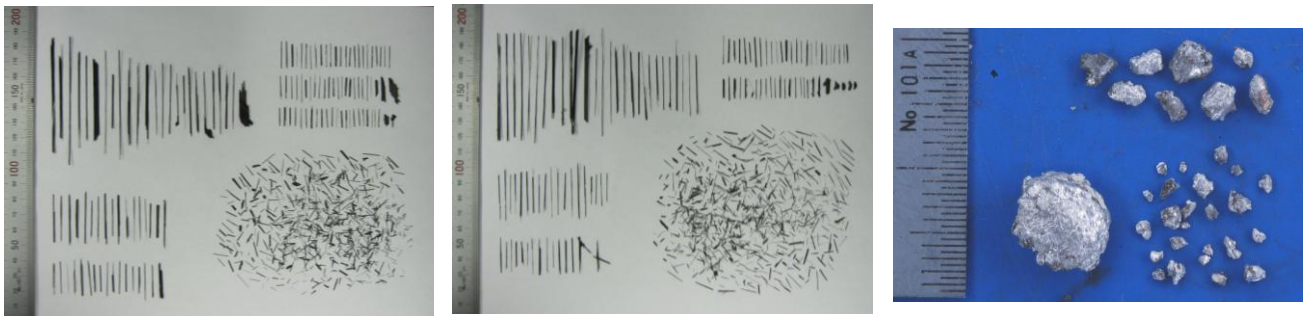

(a) Front side of target (b) Rear side of target (c) Projectile

Fig. 7. Ejecta fragments collected from test chamber (2.82 km/s).

3.4. Ejecta size distribution

As one example, photographs of ejecta fragments collected from the test chamber at an impact velocity of 2.82 km/s are shown in Fig. 7. Most of them are long and thin fragments from CFRP laminates, and a fragmented projectile was also collected from the test chamber. It seems that the projectile did not perfectly fragment. A large fragment from the projectile was also collected. Piekutowski [14] examined fragmentation process for projectile impact of aluminum sphere with a thin aluminum sheet. When the ratio of projectile diameter to target thickness was over 0.2, the threshold impact velocity for failure inside the rear surface of the sphere was 2.60 km/s. When the impact velocity was 1.39 km/s in our experiments, only large plastic deformation of the projectile was produced and the fragmentation of projectiles was not occurred. Even thought the density of CFRP targets was low, it seems that the threshold impact velocity failure inside the rear surface of the sphere was almost the same as that for projectile impact of aluminum sphere with a thin aluminum sheet.

The size (length x, width y, thickness z, in meters) of the ejecta fragments as defined in Fig. 8 was measured. Here, only the fragments from CFRP laminates were measured. Fig. 9(a) shows that the number of fragments ejected on the front side of the target increased with impact velocity. On the other hand, in Fig. 9(b) the trend in the number distribution of fragments ejected on the rear side of the target did not depend on the impact velocity. It can be seen from Fig. 9(c) that the impact velocity slightly affected the total number of fragments on the front side and the rear side. It seems from Fig. 9(d) showing the cumulative number per impact velocity that the total number of fragments is proportional to the impact velocity. We predicted that the total number of fragments would increase with impact energy, which equals the square of the impact velocity. However, a different result was obtained.

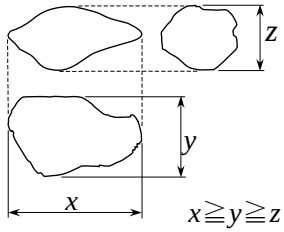

Fig. 8. Definition of ejecta fragment size.

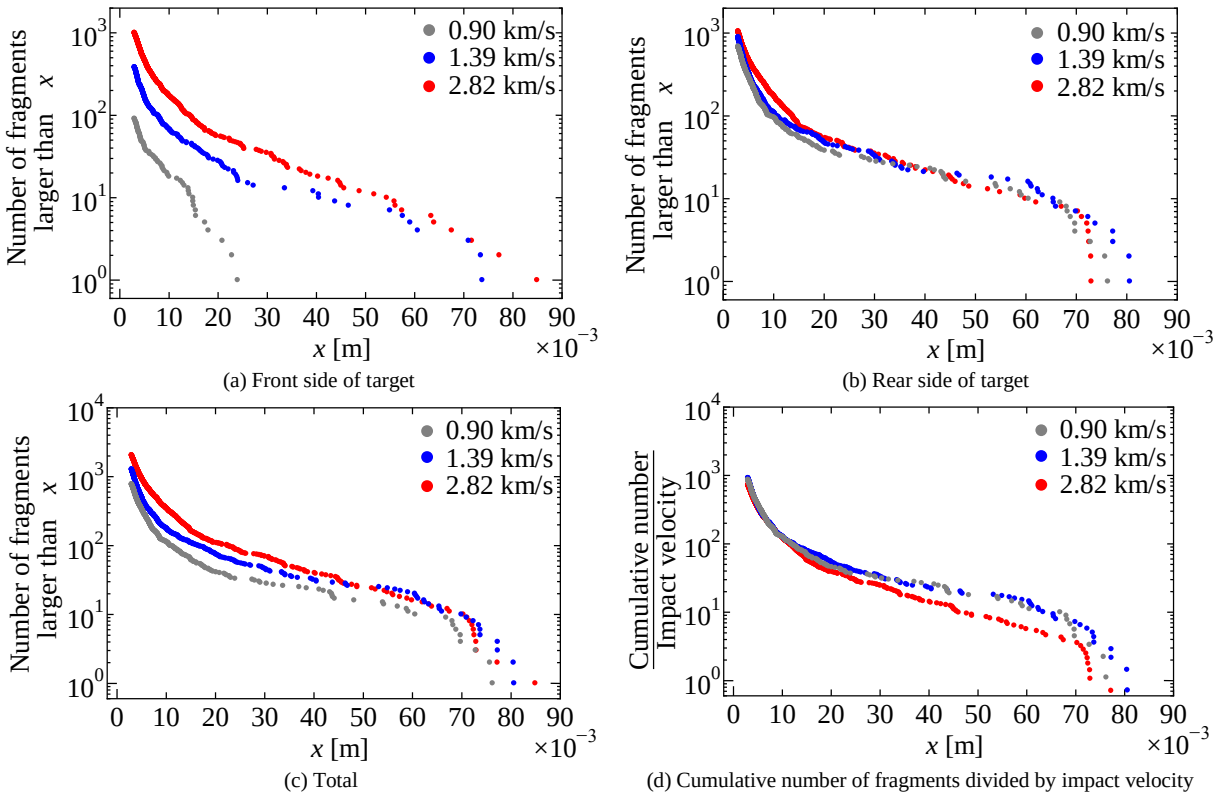

(a) Front side of target

(b) Rear side of target

(c) Total

(d) Cumulative number of fragments divided by impact velocity

Fig. 9. Cumulative number distribution of fragment length x from CFRP laminates.

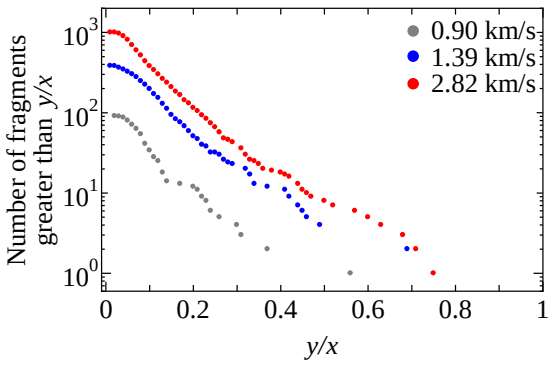

(a) Front side of target

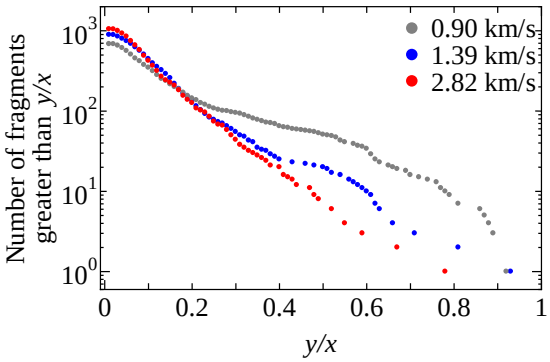

(b) Rear side of target

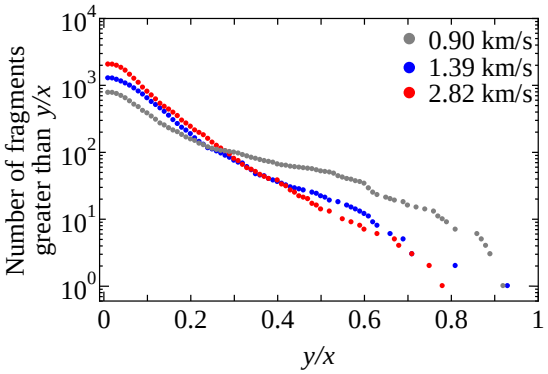

(c) Total

Fig. 10. Axial ratio of fragments from CFRP laminates.

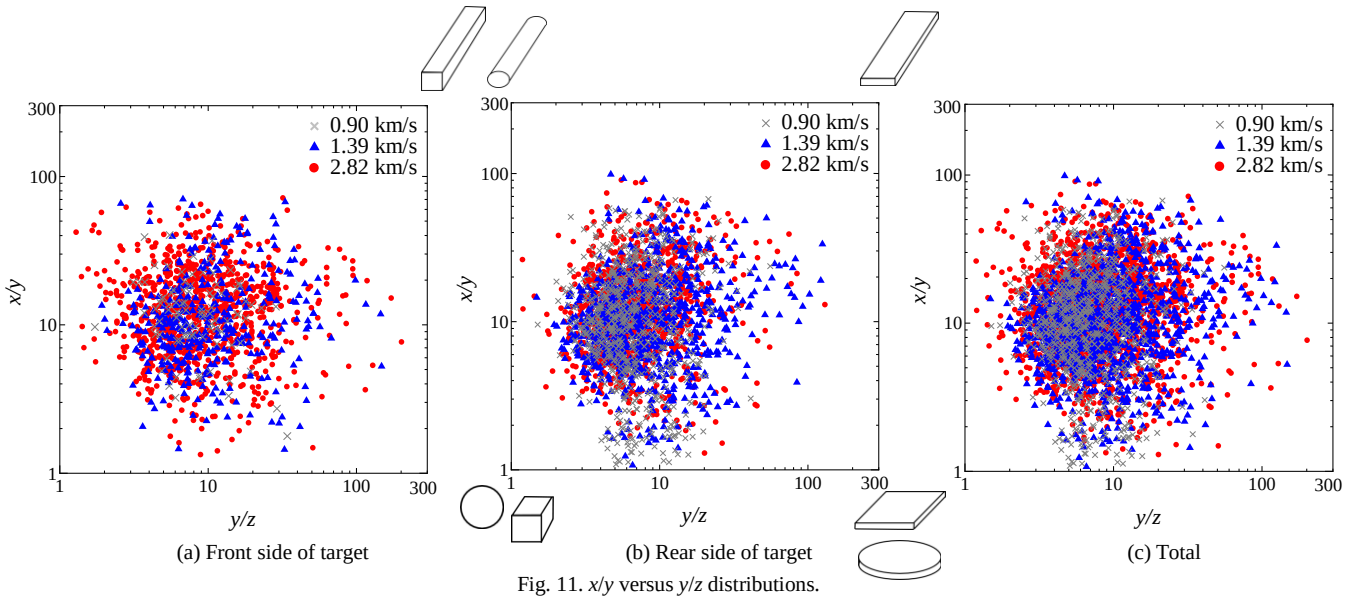

(a) Front side of target (b) Rear side of target (c) Total

Fig. 11. *x*/*y* versus *y*/*z* distributions.

The results of the axial ratios, *y*/*x*, are shown in Fig. 10(a)-(c). A *y*/*x* value of close to 0 indicates that the ejecta fragments are elongated or slender, and a *y*/*x* value of close to 1 indicates that the ejecta fragments are square or circular shapes. It was found from Fig. 10(a) that the number of fragments on the front side increased with impact velocity. At 0.90 km/s, there were more fragments of 0.2< *y*/*x* <0.9 on the rear side. When the impact velocity was not high, we predicted that plugging would occur when the projectile perforated. The fragments caused by plugging were not long and thin, and the number of fragments of 0.2< *y*/*x* <0.9 increased. As a result, the distributions of total fragments at 1.39 km/s and 2.82 km/s were almost the same. There were more fragments of 0.2< *y*/*x* <0.9 at 0.90 km/s than at 1.39 km/s and 2.82 km/s.

The shape distribution of ejecta fragments is examined in Fig. 11. A large *x*/*y* value indicates that the ejecta fragments are elongated or slender. Note *y*/*x* values were used in Fig. 10. The large *x*/*y* values mean the *y*/*x* values of close to 0. A large *y*/*z* value indicates that they are thin, and a small *y*/z value indicates that they are thick. In Fig. 11(c), *x*/*y* mainly ranged from 3 to 40 and *y*/*z* ranged from 2 to 40. This means that the shape of the ejecta fragments was slender and needle-like. Hanada *et al.* [15] reported that shape distribution of fragments from micro-satellite impact testing could be separated into two distinct groups. Objects having large *x*/*y* values are needle-like, broken up from the CFRP layers and side panels. The results of this experiment agreed with those of Hanada *et al.* When the shape distribution of ejecta fragments on the front side was compared with that on the rear side, the ejecta fragments on the rear side included more slender and needle-like shapes. The shape distribution of ejecta fragments did not depend on the impact velocity.

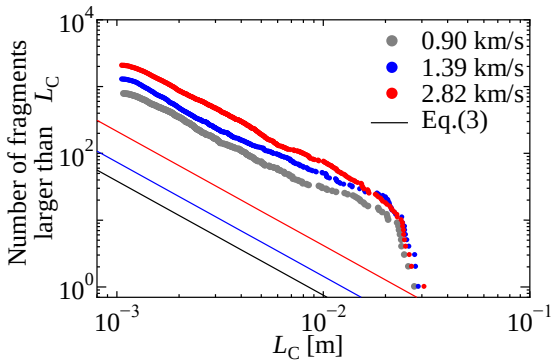

Fig. 12. Cumulative number distribution of L_C; the total number of front side and rear side of target.

3.5. Comparison with NASA's break up model

The characteristic length, $L_C=(x+y+z)/3$ in meters, of ejecta fragments was calculated using the measured ejecta fragment size, *x*, *y* and *z* in section 3.4. The characteristic length was also a parameter used in NASA's breakup model [16]. The characteristic length distribution of fragments and the area-to-mass ratio distribution of fragments were examined, and the resemblances between our results and NASA's breakup model were discussed, as described below.

In NASA's breakup model, the number of explosive fragments of size L_C or larger is governed by the following equation:

$$N(L_C) = 0.1 \cdot (M)^{0.75} \cdot (L_C)^{-1.71} \tag{3}$$

M is the total mass (in kg) of the fragments. In a non-catastrophic collision, *M* is the mass of the projectile (in kg) multiplied by the square of the impact velocity (in km/s) [16, 17] because the total mass of the fragments relates to the impact energy of the projectile. However, because of dimensional consistency, the unit of *M* is kg dividing by $(km/s)^2$ (See [17]). The average cross-section area, A_x, is expressed using L_C,

$$\left.\begin{aligned} A_x &= 0.540424 \cdot {L_C}^2, & L_C &< 0.00167 \text{ m} \\ A_x &= 0.556945 \cdot {L_C}^{2.0047077}, & L_C &\geqq 0.00167 \text{ m} \end{aligned}\right\} \tag{4}$$

When L_C<80 mm, the area-to-mass ratios, *A*/*M*, has been derived from hypervelocity impact tests for both spacecraft and upper stages as follows:

$$D_{A/M}^{\mathrm{SOC}}(\lambda_C, \chi) = N\left(\chi;\, \mu^{\mathrm{SOC}}(\lambda_C),\, \sigma^{\mathrm{SOC}}(\lambda_C)\right) \tag{5}$$

Here, *N* is the normal distribution (Gaussian distribution) function described by $\dfrac{1}{\sqrt{2\pi\sigma^2}} \exp\left(-\dfrac{(\chi-\mu)^2}{2\sigma^2}\right)$,

mean (or expectation)
$$\mu^{\mathrm{SOC}}(\lambda_C) = \begin{cases} -0.3 & \lambda_C \leqq -1.75 \\ -0.3 - 1.4(\lambda_C + 1.75) & -1.75 < \lambda_C < -1.25 \\ -1.0 & \lambda_C \geqq -1.25, \end{cases}$$

standard deviation
$$\sigma^{\mathrm{SOC}}(\lambda_C) = \begin{cases} 0.2 & \lambda_C \leqq -3.5 \\ 0.2 + 0.1333(\lambda_C + 3.5) & \lambda_C > -3.5, \end{cases}$$

$$\lambda_C = \log_{10}(L_C),$$

the variable in the distribution $\chi = \log_{10}(A/M)$

and SOC means Satellite Orbital debris Characterization impact test.

Fig. 12 shows the cumulative number distribution of the characteristic length of the ejecta fragments (the total number of front side and rear side of target). Regardless of the impact velocity, our results showed higher values than the prediction made using eq. (3). The slope of the characteristic length distribution was almost the same as the results of NASA's breakup model. By fitting the coefficient of eq. (3) to the experimental results, the following equation line can be set out in Fig. 13(a).

$$N(L_C) = 0.77 \cdot (M)^{0.75} \cdot L_C^{-1.71} \qquad \text{for the front side of the target} \qquad (6)$$

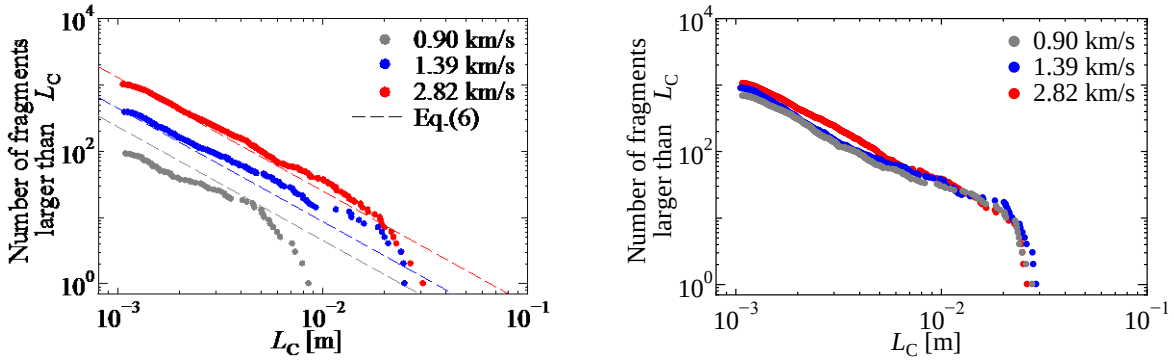

(a) Front side of target (b) Rear side of target

Fig. 13. Effect of impact velocity on cumulative number distribution of L_C.

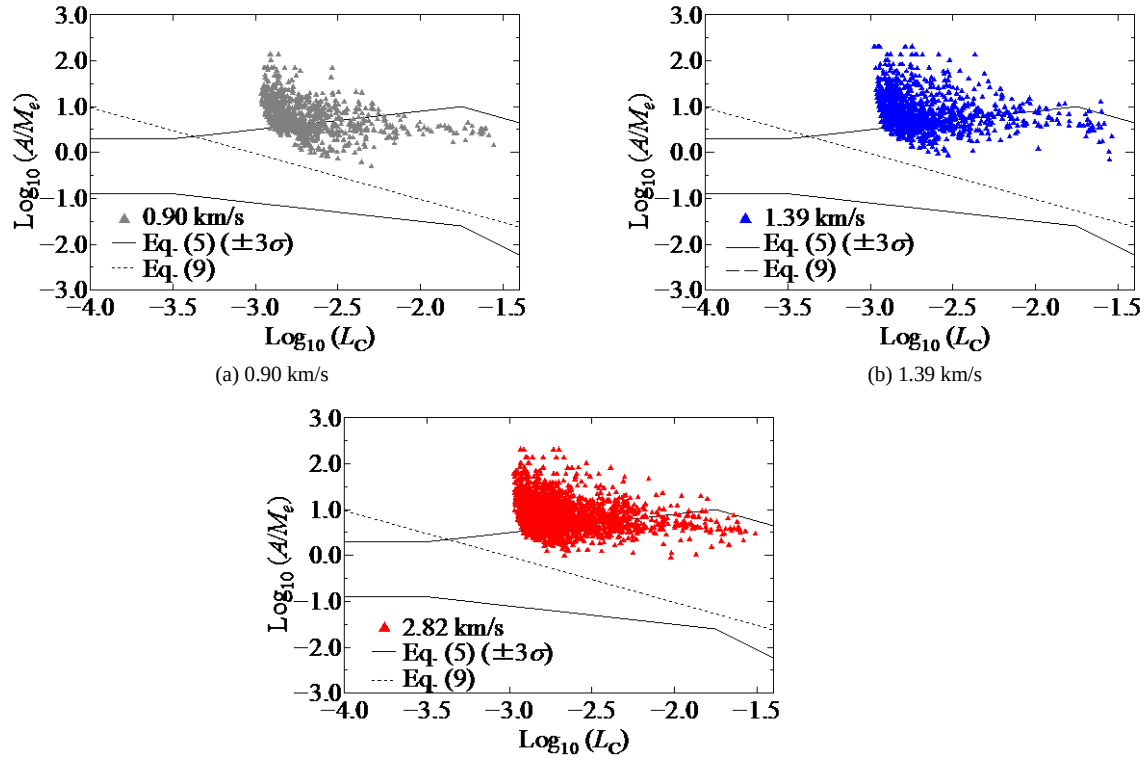

(a) 0.90 km/s (b) 1.39 km/s

(c) 2.82 km/s

Fig. 14. Comparison of area-to-mass distribution.

Eq. (6) is in good agreement with the results at 1.39 km/s and 2.82 km/s. However, Eq. (6) cannot explain the results at 0.90 km/s. The main reason for this is a change in mechanisms caused by the impact velocity of projectiles. The ejecta formation behavior at 0.90 km/s is different from that at 1.39 km/s and 2.82 km/s. It was found from Fig. 13(b) that the distribution of the characteristic length, L_C, of the ejecta fragments on the rear side did not depend on the impact velocity, nor on the distribution of the ejecta fragment length, x, as shown in Fig. 9(b). Eq. (3) means that the distribution of the characteristic length depends on the impact velocity because M was calculated using impact velocity. However, the main reason for this is still unclear, and more detailed investigation into ejecta formation of CFRP laminates is required.

Next, the relationship between area-to-mass ratio, A/M, and characteristic length, L_C, is examined. Even though eq. (4) is used for the averaged cross-sectional areas in NASA's breakup model, in this study, the averaged cross-sectional areas of fragments for arbitrary shape, A, were calculated by using

$$A = \frac{1}{3}(xy + yz + zx). \tag{7}$$

The mass of fragments was calculated by using

$$M_e = \frac{4}{3}\pi \cdot \rho \cdot x \cdot y \cdot z, \tag{8}$$

assuming that the fragments are ellipsoidal in shape. Eq. (5) is shown as a solid line in Fig. 14. Hata *et al.* [17] pointed out that a lower boundary of the area-to-mass ratio exists for plate-type fragments. When the averaged cross-sectional areas are calculated by $A=(L_C^2+2L_C \cdot z)$, the condition of the area-to-mass ratio is re-written as the following

$$A/M_e \geq 1.5/(\rho \cdot L_C) \tag{9}$$

Eq. (9) is shown by dotted lines in Fig. 14. Regardless of impact velocity, the experimental results were distributed within and above the area surrounded by ±3σ of NASA's breakup model. The main reason for this is that the density of CFRP laminates is lower than that of the aluminum alloys that were considered in NASA's model. All the experimental results were above the dotted line of eq. (9) derived by Hata *et al*. Even though Hata *et al*. proposed eq. (9) as the lower boundary for plate-type fragments, eq. (9) showed a lower boundary in this case.

4. Conclusions

The shape of the ejecta cone and debris cloud was observed using a high-speed video camera, and the ejecta size distribution of CFRP laminates collected from the test chamber was examined when the aluminum alloy spheres impacted CFRP laminates at impact velocities ranging from 0.9 to 2.8 km/s. The number of fragments ejected on the front side of the target increased with increasing impact velocity, whereas the number distribution of fragments ejected on the rear side of the target was almost the same regardless of impact velocity. The number of characteristic length was larger than the prediction using NASA's breakup model. The slope of the number distribution of characteristic length was almost the same as that of NASA's breakup model. The area-to-mass ratio distribution of ejecta fragments from CFRP laminates ranged within and above the area surrounded by ±3σ of NASA's breakup model. The lower boundary proposed by Hata *et al*. was also appropriate and could be used for the fragments of CFRP laminates.

Acknowledgements

The authors are greatly indebted to Dr. Hidehiro Hata of Kumamoto University for his valuable advice with respect to the fragmentation model. The authors are also greatly indebted to Mr. Hiroyasu Sasaki and Mr. Shunsuke Sakaguchi of nac Imaging Technology Inc. for their help with taking images using high speed cameras. This work was supported in part by a Grant-in-Aid for Scientific Research (C), KAKENHI (22560078), from the Japan Society for the Promotion of Science (JSPS).

References

[1] Hernandes, V.S., Murr, L.E., Anchondo, I.A., 2006. Experimental observations and computer simulations for metallic projectile fragmentation and impact crater development in thick metal targets, International Journal Impact Engineering 32, p. 1981.

[2] Space Systems-Test procedures to evaluate spacecraft material ejecta upon hypervelocity impact (ISO-CD-11227).

[3] Sugahara, K., Aso, K., Akahoshi, Y., Koura, T., Narumi, T., 2009. "Intact measurement of fragments in ejecta due to hypervelocity impact," Proceedings of the 60th International Astronautical Congress, IAC-09-A6.3.06.

[4] Siguier, J.M., Mandeville, J.C., 2007. Test procedures to evaluate spacecraft materials ejecta upon hypervelocity impact, Proceedings of IMechE G 221, pp. 969.

[5] Higashide, M., Nagao, Y., Kibe, S., Francesconi, A., Paverin, D., 2010. Debris impact on CFRP-Al honeycomb sandwich structure, Aerospace Technology Japan, 8, Pr_2_1-Pr_2_5.
[6] Numata, D., Ohtani, K., Anyoji, M., Takayama, K., Togami, K., Sun, M., 2008. HVI tests on CFRP laminates at low temperature, International Journal of Impact Engineering 35, p. 1695.
[7] Lamontagne, C.G., Manuelpillai, G.N., Kerr, J.H., Taylor, E.A., Rennyson, R.C., Burchell, M.J., 2001. Projectile density, impact angle and energy effects on hypervelocity impact damage to carbon fibre/peek composites, International Journal Impact Engineering 26, p. 381.
[8] Murakami, J., Hanada, T., Liou, J.-C., Stansbery, E., 2009. Two new microsatellite impact tests in 2008. NASA Orbital Debris Quarterly News 13, p. 4.
[9] Lamontage, C.G., Manuelpillai, G.N., Taylor, E.A., Tennyson, R.C., 1999. Normal and oblique hypervelocity impacts on carbon fibre/peek composites, International Journal of Impact Engineering 23, p. 519.
[10] Hazell, P.J., Cowie, A., Kister, G., Stennett, C., Cooper, G.A.. 2009. Penetration of a woven CFRP laminate by a high velocity steel sphere impacting at velocities of up to 1875 m/s, International Journal of Impact Engineering 136, p. 1136.
[11] Wicklein, M., Ryan, S., White, D.M., Clegg, R.A., 2008. Hypervelocity impact on CFRP: Testing, material modelling, and numerical simulation, International Journal of Impact Engineering 35, p. 1861.
[12] White, D.M., Taylor, E.A., Clegg, R.A., 2003. Numerical simulation and experimental charcterisation of direct hypervelocity impact on a spacecraft hybrid carbon fibre/kevlar composite structure, International Journal of Impact Engineering 29, p. 779.
[13] Nishida, M., Hayashi, K., Nakagawa, J., Ito, Y., 2012. Influence of temperature on crater and ejecta size following hypervelocity impact of aluminum alloy spheres on thick aluminum alloy targets, International Journal Impact Engineering 42, p. 37.
[14] Piekutowski, A.J., 1995. Fragmentation of a sphere initiated by hypervelocity impact with a thin sheet, International Journal Impact Engineering 17, p. 627.
[15] Hanada, T., Murakami, J., Tsuruda, Y., 2009. "Shape distribution of fragments from micro-satellite impact testing," Proceedings of Symposium On Shock Waves in Japan, pp. 23-26.
[16] Johnson, N.L. Krisko, P.H., Liou, J.-C., Anz-Meador, P.D., 2001. NASA's new breakup model of EVOLVE 4.0, Advances in Space Research 28, p. 1377.
[17] Liou, J.-C., Johnson, N. L., Krisko, P. H., Anz-Meador, P. D., 2002. The New NASA Orbital Debris Breakup Model. In: Green, S.F. et al.. editors, Dust in the Solar System and Other Planetary Systems, Pergamon, London, UK, p. 363.
[18] Hata, H., Hanada, T., Akahoshi, Y., Yasaka, T., Harada, S., 2005. Examining of the collision breakup model between geostationary orbit objects, The second report: consideration of the maximum collision velocity between geostationary earth orbit satellite, Journal of the Japan Society for Aeronautical and Space Sciences 53, p. 160. (In Japanese)